Laser-pulse sputtering of aluminum: Vaporization, boiling, superheating, and gas-dynamic effects

Andrea Peterlongo, Antonio Miotello, and Roger Kelly
Dipartimento di Fisica and Consorzio Interuniversitario Nazionale Fisica della Materia, Università di Trento, I-38050 Povo, Trento, Italy
(Received 10 June 1994)

We have developed a numerical method to describe laser-pulse sputtering of Al in a thermal regime. The irradiation consists of a single pulse of triangular form having a duration of 30 ns. The laser light is assumed to be absorbed according to a simple exponential mechanism. Heat transport in the Al is described by the heat flow equation with boundary conditions for vaporization, with or without boiling. Vaporization rates are evaluated by the Clausius-Clapeyron law and the boiling mechanism (when boiling is assumed to be possible) is implemented as soon as the vapor pressure reaches 1 atm. A critical analysis of the time scales necessary for true boiling, as well as for superheating above the boiling temperature, is made in order to understand the relevance of these phenomena with respect to particle emission from the Al surface. Moreover, on the basis of the calculated vaporization rates, it is possible to distinguish between different gas-dynamic regimes. When the rate is less than ~ 1 ML in 20 ns, the particles emerging from the surface do not achieve local thermal equilibrium, and therefore undergo free flight describable by a modified Maxwellian. When the rate is ~ 1 ML in 20 ns, a Knudsen layer forms, at the boundary of which particles achieve local thermal equilibrium and only subsequently undergo free flight. Finally, when the rate is sufficiently greater than ~ 1 ML in 20 ns, the gas dynamics of the particles leaving the Knudsen layer may be described with the gas-dynamic equations, if the density is high enough, or, otherwise, by the Boltzmann equation. Numerical results concerning the effectiveness of laser sputtering in producing craters in irradiated Al, as well as the main features of the gas dynamics (including recondensation or reflection of the gas at the Al surface), are illustrated.

PACS number(s): 47.40.−x, 47.45.−n, 51.10.+y, 61.80.−x

INTRODUCTION

Pulsed laser irradiation of metals or semiconductors involves many physical processes including the photoelectric effect; electron excitation, which induces the formation of electron-hole pairs; ionization; atom or cluster emission; and so on [1]. Moreover, when the radiation intensity is high enough, energy transferred from excited electrons to the lattice causes appreciable heating of the solid. As a consequence phase changes, vaporization, boiling, and even phase explosion [2,3] may occur. In addition, the emitted particles may interact both with the terminal part of the laser pulse and with the target surface, recondensation or reflection being possible in the latter case. Due to the complexity of these processes, approximations are necessary to describe the laser-solid interaction [4].

However, to develop a model to describe *laser ablation* (or *laser sputtering*) some approximations may be easily justified on the basis that many of the above mentioned processes are threshold processes with respect to laser-pulse specifications such as wavelength, duration, and energy density. Moreover some effects become dominant with respect to others depending on the phase (solid or liquid) of the irradiated sample, on the vaporization rate, or on the value of T_{tc}, the thermodynamic critical temperature.

In this paper we describe the main features of the thermal regime model that we have developed to account for laser sputtering of Al starting with absorption of the laser pulse and concluding with gas-dynamic processes among the emitted particles.

I. ABSORPTION OF THE LASER RADIATION

It is well known that laser light absorption may be described by an exponential law

$$I = (1 - R) I_0 \, e^{-\mu x}, \tag{1}$$

where I_0 is the intensity of the incident pulse (W/cm^2), I is the intensity at distance x beneath the surface which is located at $x = 0$, μ is the absorption coefficient, and R is the reflection coefficient. As a matter of fact μ and R may depend on the radiation frequency, on the electronic density (hence on the temperature), on the state (amorphous or crystalline), and on the presence of possible contaminants on the target surface. Moreover, as shown by Batanov *et al.* [5], when both the laser intensity (between 10^7 and 10^8 W/cm^2) and the pulse duration are high enough that the target temperature may reach a characteristic value well above the melting point, then there is indication that a metal loses the ordinary conductivity and becomes a dielectric. As a consequence the values of μ and R undergo a strong reduction, which is

TABLE I. Parameter values employed to describe laser sputtering of Al.

Melting temperature	T_m	933.5 K
Boiling temperature at 1 atm	T_b	2740 K
Latent heat of fusion	$\Delta H(T_m)$	396 J/g
Latent heat of vaporization at T_b	$\Delta H(T_b)$	10 500 J/g
Solid phase density	ρ	2.7 g/cm^3
Liquid phase density	ρ	2.7 g/cm^3
Solid phase specific heat	c	0.94 J/g K
Liquid phase specific heat	c	0.94 J/g K
Solid phase thermal conductivity	$K_{\rm sol}$	2.25 J/s cm K
Liquid phase thermal conductivity	$K_{\rm liq}$	1 J/s cm K
Reflection coefficient ($\lambda \approx 600$ nm)	R	0.79
Absorption coefficient	μ	5.0×10^5 cm^{-1}
Specific heat ratio	γ	5/3

shown by Martynyuk [2] to have particular importance for phase explosion.

While recognizing the complicated effects which may occur in laser-surface interactions, we have decided to describe a kind of ideal sample in which μ and R may be considered temperature independent (see Table I). Moreover, due to the very low density of the emitted gas particles with respect to the solid or liquid density, we also neglect any form of laser-gas interaction. (This simplification is quite reasonable as far as target temperature is concerned, but less so for gas-dynamic effects.)

When dealing with a laser pulse in the nanosecond regime it is possible to consider as instantaneous the electron-lattice coupling even if, at first, the energy absorbed from the pulse increases only the kinetic energy of the free carriers (metals) or the number of electron-hole pairs (materials with a band gap). In fact, charge carriers may reach thermal equilibrium in about 10^{-14} s, but, due to electron-phonon interactions which seem to have a positive feedback, there is also a very fast energy transfer to the lattice which is complete in about 10^{-12} s [1]. The form of the laser-pulse intensity I_0 adopted in our simulation will be taken as "triangular" [6]:

$$I_0 = \begin{cases} I_t\, t\ , & 0 \le t \le \tau_l/2 \\ 2\, I_t\, (\tau_l/2) - I_t\, t\ , & \tau_l/2 \le t \le \tau_l \\ 0\ , & t \ge \tau_l\ , \end{cases} \qquad (2)$$

where τ_l is the duration of the pulse (30 ns in the present case).

II. HEAT TRANSPORT AND PHASE TRANSITIONS

A. Underlying assumptions

To describe heat flow we make use of the heat flow equation in one-dimensional form, as is appropriate to many experimental conditions [7]:

$$c(T)\,\rho(T)\frac{\partial T}{\partial t} = \frac{\partial}{\partial x}\left(K(x,T)\frac{\partial T}{\partial x}\right) + S(x,t), \qquad (3)$$

where T, $c(T)$, $\rho(T)$, and $K(x,T)$ are, respectively, temperature, specific heat, mass density, and thermal conductivity (units as in Table I) and $S(x,t)$ is the heat source term given by Eq. (1) multiplied by μ. The quantities c, ρ, and K will be subsequently assumed to be temperature and space independent.

The heat flow equation derived from Fourier's law

$$J = -K\nabla T \qquad (4)$$

is subject to some restrictions when applied to heat transients where temperature gradients may be very large ($10^6 - 10^7$ K/cm). In particular, according to Harrington [8], Eq. (3) holds only if the temperature gradient may be considered constant over at least ten mean free paths of the heat carriers (one mean free path is about 20 nm in Al at room temperature), with higher temperature derivatives otherwise being needed to describe the heat flow. We have checked this condition during our simulations and it is indeed satisfied in the nanosecond regime with an energy density of the order of 3.0–4.0 J/cm^2.

Neglecting radiative loss from the surface ($x = 0$) and considering the x axis as directed toward the sample interior, then the following boundary conditions may be assumed:

$$T(x,t)|_{t=0} = T_{\rm amb} \qquad (5a)$$

and

$$T(x,t)|_{x\to\infty} = T_{\rm amb}, \qquad (5b)$$

where $T_{\rm amb}$ is the ambient temperature ($T_{\rm amb} = 298$ K). For $T < T_m$ (T_m is the equilibrium melting temperature of the irradiated sample, 934 K in the case of Al), and with vaporization neglected, one also requires the following surface condition to avoid energy loss [9]:

$$J_T|_{x=0,t} = -K\left.\frac{\partial T}{\partial x}\right|_{x=0,t} = 0, \qquad (6)$$

where J_T is the total flux.

To consider solid-liquid or liquid-solid transitions, two boundary conditions are required at the interface where the phase transition occurs. The first of these is an energy balance:

$$\rho\,\Delta H_m(T_{\rm tr})\,v_{\rm int} = K_{\rm sol}\left.\frac{\partial T}{\partial x}\right|_{x_{\rm int}^+} - K_{\rm liq}\left.\frac{\partial T}{\partial x}\right|_{x_{\rm int}^-}, \qquad (7)$$

where $T_{\rm tr}$ is the temperature at which the transition takes place, $\Delta H_m(T_{\rm tr})$ is the heat of melting at $T = T_{\rm tr}$, and $v_{\rm int}$ is the solid-liquid interface velocity. Moreover, the thermodynamics of crystal growth requires that $v_{\rm int}$ be a function of $T_{\rm tr} - T_m$,

$$v_{\rm int} = f(T_{\rm tr} - T_m), \tag{8}$$

where f is determined by crystal growth thermodynamics [9].

It has been shown that in an Al film irradiated in the picosecond regime, superheating of the solid by 350 K (i.e., to 1284 K) has a maximun duration of the order of 1 ns [10]. One may therefore argue that, when dealing with Al irradiated with a 30 ns pulse, superheating above T_m plays no role. Another factor in this regard is the presence of a high thermal gradient between the surface and the interior. Moreover it may be shown that the role of undercooling of the liquid may also be neglected [9]. We thus have $T_{\rm tr} \simeq T_m$ and only Eq. (7) need be taken into account.

Equation (6) holds only if no vaporization occurs. However, for high enough temperatures (here taken as $T > T_m$), vaporization will be important and so Eq. (6) is no longer valid. During vaporization the surface recedes with velocity v_r. It is, however, still possible to label its position with $x = 0$ if one chooses a reference frame moving with the receding surface. Then, neglecting mass accumulation and temperature dependence, Eq. (3) becomes

$$c\rho \frac{\partial T}{\partial t} = K \frac{\partial^2 T}{\partial x^2} + c\rho v_r \frac{\partial T}{\partial x} + S(x,t). \tag{9}$$

At the surface the total flux is

$$\begin{aligned} J_T|_{x=0,t} = &-K\frac{\partial T}{\partial x}\bigg|_{x=0,t} \\ &-[c(T - T_{\rm amb}) + \Delta H_m(T_m)]\rho v_r \\ &-\Delta H_v(T)\rho v_r \ , \end{aligned} \tag{10}$$

with $-K(\partial T/\partial x)|_{x=0,t} = 0$. The first term on the right is zero because there is no heat conduction through the surface. The second term describes the total energy of the escaping particles and is already taken into account with Eq. (9). $\Delta H_v(T)$ is the heat of vaporization that we assume, as a first approximation, equal to the value at T_b, the boiling temperature at 1 atm.

A simple way to compute v_r as a function of temperature is to consider what happens when a liquid is in thermal equilibrium with its saturated vapor. In this case the number N_v of particles vaporizing per unit time and area is

$$N_v = \frac{p}{(2\pi k_B T m)^{1/2}} C_S, \tag{11a}$$

where p is the gas pressure, k_B is the Boltzmann constant, m is the particle mass, and C_S is the sticking coefficient ($C_S \simeq 1$) [11,12]. One may assume that Eq. (11a) also holds in a nonequilibrium situation as when particles are emitted into vacuum thus yielding

$$v_v = \frac{p}{\rho(2\pi k_B T/m)^{1/2}} C_S, \tag{11b}$$

where v_v is the vaporization velocity. (Note that we allow a nonzero v_v at all temperatures.) The relation between the equilibrium vapor pressure and the temperature may be computed from the Clausius-Clapeyron equation in the limit $V_{\rm liq} \ll V_{\rm gas}$, $V_{\rm liq}$ and $V_{\rm gas}$ being the molar volume of liquid and gas, respectively. We assume the inequality $T < T_{\rm tc}$, where $T_{\rm tc}$ is (as before) the thermodynamic critical temperature, and write

$$p = p_b \exp\left\{\frac{\Delta H_v(T_b)\, m}{k_B}\left(\frac{1}{T_b} - \frac{1}{T}\right)\right\}, \tag{12}$$

where p_b is 1 atm.

As will be explained in Sec. III C 3, when v_v reaches a threshold value of about $v_v^\star \simeq (2.8 \times 10^{-8}\ {\rm cm})/(20\ {\rm ns}) = 1.4$ cm/s, then gas-dynamic effects associated with the Knudsen layer lead to a strong backstreaming which must be taken into account by introducing a coefficient $C_{\rm bs}$. As a consequence the velocity at which the surface recedes is given by

$$v_r = v_v\,(1 - C_{\rm bs}). \tag{13}$$

Concerning $C_{\rm bs}$, lacking better information and in order to ensure the continuity of v_r as a function of temperature, we arbitrarily assign it a value given by

$$C_{\rm bs} = C_{\rm bs0} \exp\left\{-\frac{v_v^\star - v_v}{v_v}\right\}, \tag{14}$$

where $C_{\rm bs0}$, the *backstreaming coefficient*, will be deduced in Appendix A [Eq. (A8)]. Equation (14) applies for $0 < v_v \le v_v^\star$ if v_v *has not* already reached $v_v^\star$; otherwise, for $v_v \le v_v^\star$ and if v_v *has* already reached $v_v^\star$ or else for $v_v \ge v_v^\star$, we have the equality $C_{\rm bs} = C_{\rm bs0}$.

What about boiling? When the surface temperature reaches T_b, then the vapor pressure equals the external pressure p_b. As a consequence, bubble nucleation may occur in the bulk, bubbles themselves may move toward the surface, and the vaporization rate may be enhanced. At the same time the temperature of the sample will tend to assume a constant value.

But is the above mentioned process what actually happens when using laser pulses in the nanosecond regime? As a matter of fact, if the time in which heat is deposited on the sample by a laser pulse is too short for bubbles to nucleate, then a significant superheating above T_b will occur, with the temperature finally reaching $T_{\rm tc}$. Alternatively, if the velocity at which the surface recedes is high enough, then nucleation cannot in any case occur and again superheating will occur. Since the transition from simple vaporization to boiling needs a characteristic time τ_b of about $10^{-9} - 10^{-8}$ s for a liquid dielectric and $10^{-13} - 10^{-11}$ s for metals [13], then we do not expect boiling in the picosecond regime while in the nanosecond regime the question is still open to a definitive answer. This is why we will present in Sec. II B results for both situations, boiling and superheating.

TABLE II. Main results obtained during the heating phase by irradiating an Al sample with a single 30 ns laser pulse. A recondensation boundary condition is assumed for the KL.

Without boiling					
Energy density (J/cm^2)	Start of liquid phase (ns)	Duration of liquid phase at the surface (ns)	Maximum temperature at the surface (K)	Maximum velocity of surface recession v_r (cm/s)	Crater depth per pulse (nm)
3.00	8.3	97	2588	0.7	4.9×10^{-2}
3.10	8.0	104	2679	1.0	7.7×10^{-2}
3.20	7.9	118	2769	1.5	1.2×10^{-1}
3.30	7.7	125	2859	2.2	1.7×10^{-1}
3.50	7.5	131	3039	4.3	3.5×10^{-1}
3.70	7.3	145	3217	7.8	6.4×10^{-1}
With boiling at 2740 K					
Energy density (J/cm^2)	Start of boiling (ns)	Duration of boiling (ns)	Maximum temperature at the surface (K)	Maximum velocity of surface recession v_r (cm/s)	Crater depth per pulse (nm)
3.00			2588	0.7	4.9×10^{-2}
3.10			2679	1.0	7.7×10^{-2}
3.20	18.5	2.5	2740	44.9	8.2×10^{-1}
3.30	17.2	4.5	2740	127.7	4.1
3.50	16.0	6.8	2740	262.3	12.3
3.70	15.3	8.0	2740	287.6	21.5

B. Numerical results

In our study first we have used the simple vaporization model given by Eq. (13) even to describe superheating above T_b. Then we have examined the consequences of boiling by implementing a boiling mechanism as soon as T reaches T_b. The temperature of the surface is kept constant and the excess energy deposited in the bulk by the laser pulse is completely used to enhance vaporization, no energy being spent in the heating of the emitted particles.

On the basis of the above arguments, keeping the duration of the laser pulse equal to 30 ns and with the pulse having a triangular form as in Eq. (2), simulations were performed by considering different values of the laser-pulse energy density E_l. These allowed us to establish the energy density threshold for T_b to be reached as lying between 3.15 and 3.20 J/cm^2.

We report on six typical responses of the irradiated samples for energy densities below and above this threshold, namely, E_l = 3.00, 3.10, 3.20, 3.30, 3.50, and 3.70 J/cm^2 (Figs. 1–4 and Table II). A comparison between the maximum values of v_r when a boiling mechanism is operative (for example, v_r = 45 cm/s for $E_l = 3.20\,J/cm^2$ and $v_r = 128$ cm/s for $E_l = 3.30\,J/cm^2$ as in Fig. 3) as opposed to those when it is not operative ($v_r = 1.5$ cm/s for $E_l = 3.20\,J/cm^2$ and $v_r = 2.2$ cm/s for $E_l = 3.30\,J/cm^2$ as in Fig. 4) show that boiling is important in enhancing the efficiency of laser sputtering. A further indication of this importance is given by the crater depths as summarized in Table II.

III. GAS DYNAMICS

A. Collision-free flow

For particle emission by a thermal mechanism the velocity distribution of the particles must be given by a Maxwellian restricted to v_x positive [14,15]:

$$f_S^+ = n_S \left(\frac{m}{2\pi k_B T_S}\right)^{3/2} \frac{E_I^{j/2-1}}{\Gamma(j/2)\,(k_B T_S)^{j/2}} \times \exp\left\{-\frac{1}{k_B T_S}\left[\frac{m}{2}(v_x^2+v_y^2+v_z^2)+E_I\right]\right\} \quad \text{for } v_x \geq 0,\ -\infty < v_y, v_z < +\infty. \quad (15)$$

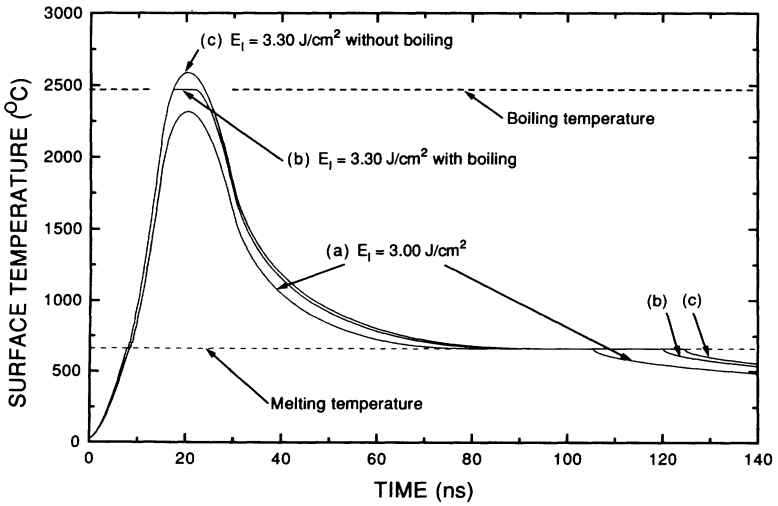

FIG. 1. Surface temperature of an Al sample irradiated with a single 30 ns laser pulse with energy density equal to 3.00 J/cm^2 for (a) and to 3.30 J/cm^2 for (b) and (c). In (b) it has been assumed that boiling is *possible* on the relevant time scale 30 ns while in (c) it has been assumed to be *impossible*.

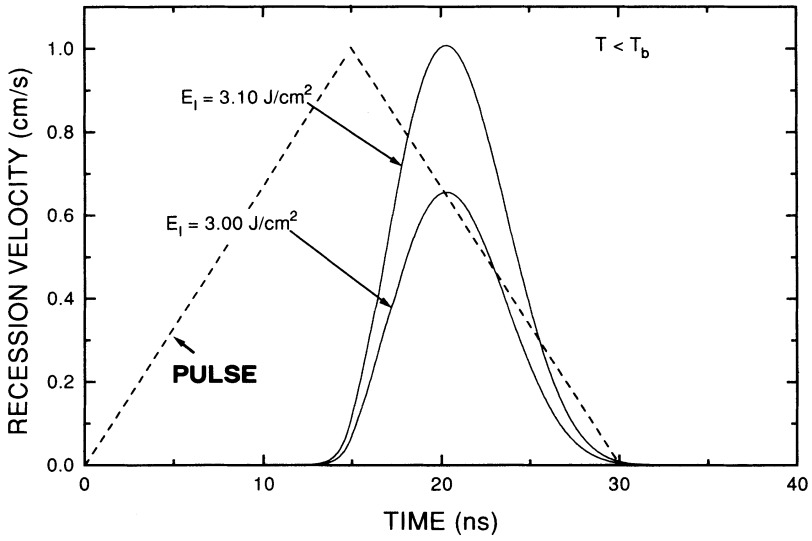

FIG. 2. Velocity of Al surface recession, v_r, for two energy densities of the laser pulse which give maximum temperatures below T_b. A recondensation boundary condition is assumed for backstreaming particles whenever a KL is present.

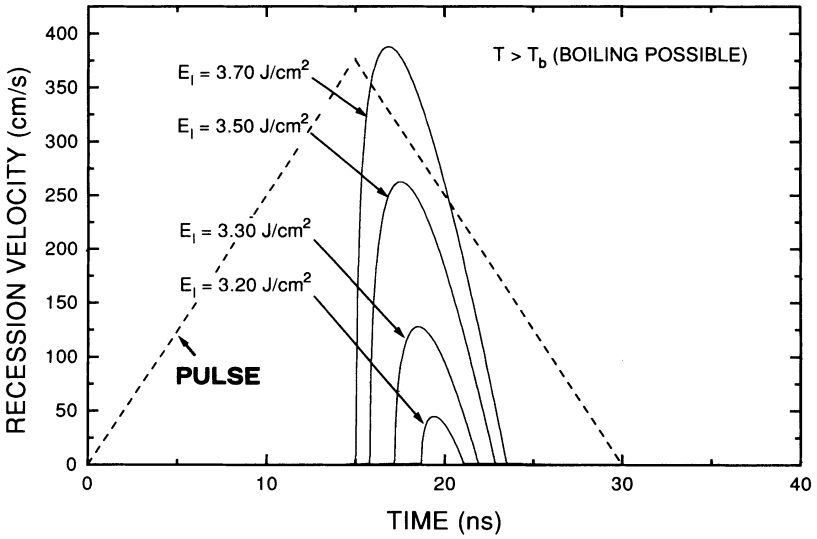

FIG. 3. Velocity of Al surface recession, v_r, for four energy densities of the laser pulse which give maximum temperatures above T_b. Here it is assumed that boiling is *possible* on the relevant time scale 30 ns. A recondensation boundary condition is assumed for backstreaming particles whenever a KL is present.

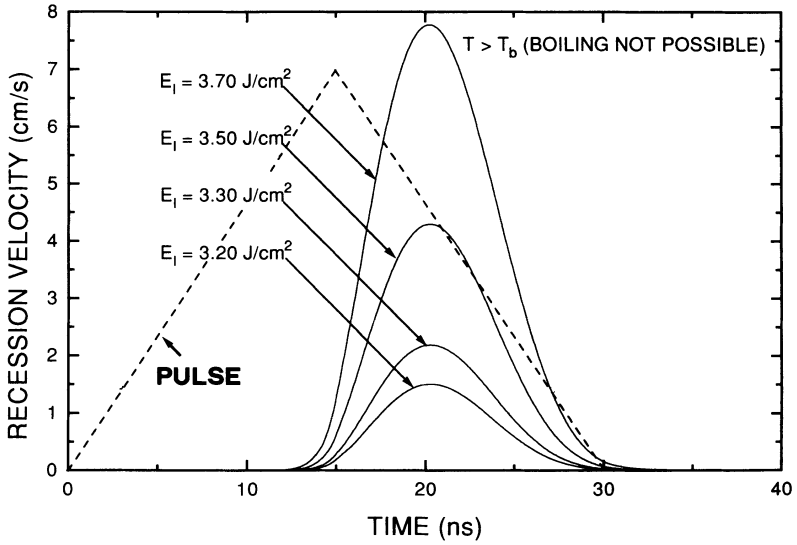

FIG. 4. Velocity of Al surface recession, v_r, for four energy densities of the laser pulse which give maximum temperatures above T_b. Here it is assumed that boiling is *impossible* on the relevant time scale 30 ns. A recondensation boundary condition is assumed for backstreaming particles whenever a KL is present.

Here E_I is the total internal energy of the gas, j is the number of internal degrees of freedom, Γ is the gamma function, and T_S and n_S are, respectively, the temperature and the number density of the gas at the surface. The pre-exponential term $E_I^{j/2-1}$ serves to ensure that $\langle E_I \rangle$ deduced from Eq. (15) assumes a thermodynamically correct value given by $(j/2)k_B T_S$ [15,16]. A kind of "center of mass velocity" is given by

$$\langle v_x \rangle = \frac{\int_0^\infty \int_{-\infty}^{+\infty} \int_{-\infty}^{+\infty} v_x f_S^+ \, dv_x \, dv_y \, dv_z}{\int_0^\infty \int_{-\infty}^{+\infty} \int_{-\infty}^{+\infty} f_S^+ \, dv_x \, dv_y \, dv_z} = \left(\frac{2 k_B T_S}{\pi m} \right)^{1/2} . \quad (16)$$

For low rates of vaporization, the density of the particles is so low that a collision is an unusual event: the particles therefore undergo a so-called *collision-free flow* [14,17]. In this situation each particle keeps its original velocity and, in the limit $t \gg \tau_l$, where τ_l is (as before) the duration of the laser pulse, the position of each particle emitted at the instant t_l is given by

$$x = v_x (t - t_l) \simeq v_x t,$$

where $0 < t_l < \tau_l$. The corresponding velocity distribution may be approximated by

$$f_D^+(v_x, v_y, v_z) = n_g(x,t) \left(\frac{m}{2\pi k_B T_S} \right) \frac{E_I^{j/2-1}}{\Gamma(j/2)(k_B T_S)^{j/2}} \delta(x - v_x t) \times \exp\left\{ -\frac{1}{k_B T_S} \left[\frac{m}{2}(v_y^2 + v_z^2) + E_I \right] \right\} , \quad (17)$$

where n_g is the gas number density and D stands for Dirac.

Collision-free flow is characterized by the fact that the ratio $T_\parallel / T_\perp$ undergoes a strong reduction termed *kinematic cooling* for $x \gg 0$ or $t \gg \tau_l$ due to the fact that $\langle (v_x - \langle v_x \rangle)^2 \rangle$ (which is proportional to $T_\parallel$) goes to 0 [18]. Here $T_\parallel$ and $T_\perp$ are, respectively, the temperature parallel and perpendicular to the direction of the flow.

B. The Knudsen layer

We have not yet commented on the problem that thermally emitted particles, described by Eq. (15), are not really in equilibrium. Equilibration occurs in the first few collisions near the surface in a region termed the Knudsen layer (KL). At the "boundary" of the KL the velocity distribution takes on the form of a displaced Maxwellian

$$f_K^\pm = n_K \left(\frac{m}{2\pi k_B T_K} \right)^{3/2} \frac{E_I^{j/2-1}}{\Gamma(j/2)(k_B T_K)^{j/2}} \times \exp\left\{ -\frac{1}{k_B T_K} \left[\frac{m}{2} \left[(v_x - u_K)^2 + v_y^2 + v_z^2 \right] + E_I \right] \right\} \quad \text{for } -\infty < v_x, v_y, v_z < +\infty, \quad (18)$$

where n_K, u_K, and T_K are, respectively, the number density, the flow velocity, and the temperature at the "boundary" of the KL. Conditions of local equilibrium then hold. (In fact a KL is really infinitely thick, but is nearly fully developed after only 2–3 mean free paths [19,20]. This is why we speak of a boundary.)

There are now two possibilities. If the sticking coefficient for backstreaming particles is given by $C'_S = 1$, one has a *recondensation boundary condition*, as described in Appendix A. If, on the other hand, the sticking coefficient is given by $C'_S = 0$, one has a *reflection boundary condition*, as described in Appendix B.

In either case the important result is that *jump conditions* emerge. They are expressed in terms of the ratios T_K/T_S and ρ_K/ρ_S as in Eqs. (A4), (A5), (B4), and (B5), ρ_K and ρ_S being mass densities corresponding to n_K and n_S.

C. Beyond the Knudsen layer

1. The Boltzmann equation

A rigorous study of the dynamical behavior of particles emitted as in Eq. (15) may be done by using the well known Boltzmann equation [21]

$$\frac{\partial f_B}{\partial t} + \nabla f_B \, \mathbf{v} + \sum_i F_i \frac{\partial f_B}{\partial v_i} = \Delta_C f_B,$$

$$\Delta_C f_B = \int_{\mathbf{v}_1} \int_{\mathbf{v}'} \int_{\mathbf{v}'_1} v_{\rm rel} (f'_B f'_{B1} - f_B f_{B1}) \sigma d\mathbf{v}_1 \, d\mathbf{v}' \, d\mathbf{v}'_1. \quad (19)$$

Here $f_B(\mathbf{x}, \mathbf{v}, t)$ is the Boltzmann velocity distribution, F_i is the force per unit mass acting on each particle, σ is the cross section for an *elastic* binary collision, $\mathbf{v}, \mathbf{v}_1, \mathbf{v}', \mathbf{v}'_1$ are, respectively, the velocities of two colliding particles before and after the collision, and $v_{\rm rel}$ is given by $v_{\rm rel} = |\mathbf{v} - \mathbf{v}_1| = |\mathbf{v}' - \mathbf{v}'_1|$. Moreover the index i assumes the meaning of x, y, z.

Equation (19) holds under very weak restrictions. However, to solve it the cross section must be known, and to take into account Eq. (15) as the boundary condition a Monte Carlo calculation must be performed, which is very expensive in CPU time [18,22].

2. The flow equations

For most purposes one is not interested in the time evolution of f_B itself but in that of the mean values of a physical quantity $\chi(x, v, t)$, which will depend on the position and velocity of one single particle. The Enskog equation may then be used. There are then no more constraints than those for the Boltzmann equation [21,23]. When dealing with average $\chi(x, v, t)$ functions during each binary collision, the Enskog equation has the form

$$\frac{\partial}{\partial t}(n_g \langle \chi \rangle) + \sum_i \frac{\partial}{\partial x_i}(n_g \langle v_i \chi \rangle) = n_g \langle D\chi \rangle, \quad (20)$$

where $D\chi$ is given by

$$D\chi = \frac{\partial \chi}{\partial t} + \sum_i v_i \frac{\partial \chi}{\partial x_i} + \sum_i F_i \frac{\partial \chi}{\partial v_i},$$

index i (as before) assumes the meaning of x, y, z, and x_x (for example) is equivalent to x. Moreover when χ is equal to the particle mass m, or to the linear momentum $m\mathbf{v}$, or to the energy of two colliding particles $(1/2)\,m\mathbf{v}^2$, then Eq. (20) yields the mass continuity equation, the Euler equation, and the energy conservation equation, respectively. However, these three equations form a system that is not complete, i.e., there are more unknowns than equations.

A complete three equation system, that is, the *gas-dynamic equations*, may be obtained via the Chapman-Enskog perturbation method [24], holding when the collisional term of the Boltzmann equation ($\Delta_C f_B$) is preponderant with respect to the dynamical terms (the remainder). They are as follows: the continuity equation

$$\frac{\partial \rho_g}{\partial t} + \nabla(\rho_g\,\mathbf{u}) = 0, \tag{21a}$$

the Euler equation

$$\frac{\partial}{\partial t}(\rho_g\,u_\alpha) + \sum_i \frac{\partial}{\partial x_i}(\rho_g\,u_\alpha\,u_i) + \frac{\partial p}{\partial x_\alpha} = 0, \tag{21b}$$

and the energy conservation equation

$$\frac{\partial}{\partial t}\left[\rho_g\left(\frac{1}{2}\mathbf{u}^2 + \mathcal{E}\right)\right]$$

$$+\sum_i \frac{\partial}{\partial x_i}\left[\rho_g\,u_i\left(\frac{1}{2}\mathbf{u}^2 + \mathcal{E} + \frac{p}{\rho_g}\right)\right] = \sum_i \frac{\partial \Phi_i}{\partial x_i}. \tag{21c}$$

Here u_α ($\alpha = x, y, z$) are the three components of the flow velocity $\mathbf{u}$, the quantities p, ρ_g, and $\mathcal{E}$ are, respectively, the pressure, mass density, and internal energy per unit mass of the gas, and Φ is the external (laser) heat input into the gas.

In the adiabatic expansion approximation we have $\sum_i \partial\Phi_i/\partial x_i = 0$, while for a perfect gas one can in general write

$$p = (\gamma - 1)\,\rho_g\,\mathcal{E}, \tag{22}$$

where $\gamma = C_p/C_V$ is the specific heat ratio. Equation (21c) now yields the Poisson equation

$$\frac{p}{p_0} = \left(\frac{\rho_g}{\rho_{g0}}\right)^\gamma, \tag{23a}$$

where p_0 and ρ_{g0} are, respectively, the pressure and mass density of the gas at some arbitrary position and time. In effect, the use of Eqs. (21a), (21b), plus (23a) continues to conserve all three of mass, momentum, and energy. Using the adiabatic sound velocity $a = (\gamma p/\rho_g)^{1/2}$, Eq. (23a) may be rewritten as

$$\frac{\rho_g}{\rho_{g0}} = \left(\frac{a}{a_0}\right)^{2/(\gamma-1)}. \tag{23b}$$

From Eqs. (23a) and (23b) follows the relation

$$\frac{\partial p}{\partial x} = a^2\,\frac{\partial \rho_g}{\partial x}. \tag{23c}$$

3. *Unsteady adiabatic expansion*

If the density of the gas at the boundary of the KL is high enough, then the particles enter into a so-called *unsteady adiabatic expansion* (UAE), which is well described by the gas-dynamic equations [4]. However, it should be noticed that at the expansion front, even in the presence of an UAE, the number density of the particles is so low that only the Boltzmann equation can give a good description of the gas. The threshold for the UAE corresponds roughly to an emission rate of about 1 ML in 20 ns, which [neglecting the difference between v_v and v_r seen in Eq. (13)] is equivalent to $v_v^\star \simeq (2.8\times10^{-8}$ cm)/(20 ns)=1.4 cm/s for the recession velocity of the surface [14].

If the vaporization rate is below $v_v^\star$, then gas-dynamic effects do not occur at all, except possibly for formation of the KL, and we neglect them. On the other hand, as soon as the vaporization rate reaches $v_v^\star$ at time $t = t_v^\star$ we make full use of Eqs. (21a), (21b), and (23a). The equations were integrated numerically in one-dimensional form by following the Godunov scheme [25] with the KL jump conditions and $M = 1$ as boundary conditions (see Appendix C). Here M is the *Mach number*, given by $M = u/a$ for a one-dimensonal flow. Moreover, since the crater depth is relatively small compared to the distance scale of gas dynamics, we neglect the motion of the receding surface [v_r as in Eq. (13)] in connection with the gas dynamics.

Concerning Eq. (23a), the logical choices for p_0 and ρ_{g0} are obviously p_K and ρ_K. However, as the ratio p/ρ_g^γ evaluated at the KL boundary is a monotonically decreasing function of T_K, which is in turn related to T_S, we must face the problem that the flow is not actually barotropic, i.e., the pressure is not a function only of the density, and that Eq. (23a) gives only a local description of energy conservation. As a result, p/ρ_g^γ varies with x and t. Nevertheless we have assumed that a good approximation of energy conservation still holds if during the emission phase p/ρ_g^γ assumes, for each value of t, a unique value for the whole gas equal to that computed at the boundary of the KL. When the vaporization rate goes below the threshold for KL formation we assume that p/ρ_g^γ retains a constant value. That is, we neglect heat loss to the target surface.

Two extreme boundary conditions may be analyzed when considering gas-dynamic processes at an emitting surface: *recondensation* with sticking coefficient $C_S' = 1$ and *reflection* with $C_S' = 0$. Obviously intermediate cases are possible, $1 > C_S' > 0$, but we do not consider them.

The backstreaming within the KL was implicitly taken into account by the parameter $C_{\rm bs}$ as in Eq. (14) and in Appendix A. There is otherwise no return of particles to the surface during the emission process. However, when the emission ends the KL is instantaneously removed. Particles can now scatter towards the surface, and it is supposed that C_S' is equal to 1 when recondensation occurs and 0 when reflection occurs.

D. Numerical results

In Fig. 5 we report the results obtained using a recondensation boundary condition, energy density of 3.70 J/cm^2, and three values of t. Three different aspects are illustrated.

Emission leading to a UAE begins at $t = t_i = t_v^\star = 14.9$ ns and we consider in curve (a) the gas density and flow velocity when the surface temperature reaches its maximum at t=20.3 ns. The gas density has its maximum at the KL boundary ($\rho_K = 200\,\mu$g/cm^3) and drops to 0 well away from the surface. The flow velocity of the gas at the KL boundary is $u_K = 1051$ m/s, but increases with distance. According to previous analytical work, u at the expansion front should be a maximum, given by $\hat{u} = 4u_K$ for atoms with $\gamma = 5/3$ [14,26,27]. The observed discrepancy, i.e., that the flow velocity reaches a maximum slightly before the expansion front, is due to the fact that near the front the density is so low that the numerical method and rounding error play a significant role. More accurate results may be obtained by decreasing the time and spatial step lengths, a procedure which, however, implies a heavy increase in the CPU expense.

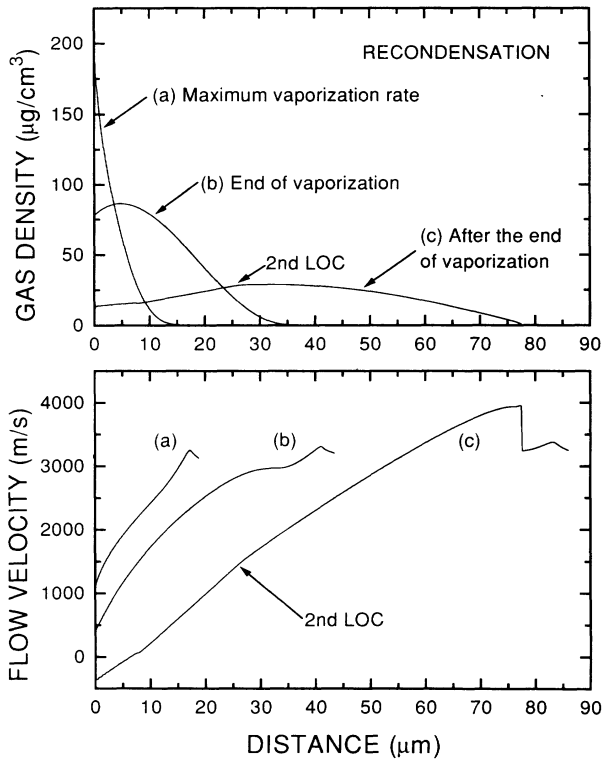

FIG. 5. Profiles of gas density and flow velocity for an energy density equal to 3.70 J/cm^2, three values of t, a recondensation boundary condition, and the assumption that boiling is *not possible*. Emission leading to a UAE is found to begin at a time threshold $t_i = t_v^\star = 14.9$ ns, when we have $v_v = v_v^\star$ and $T = 2693$ K. Curve (a) corresponds to the time when the surface temperature is at its maximum, namely, $t = 20.3$ ns. Curve (b) is for the time at the end of the emission, namely, $t_f = t_v^\star = 27.4$ ns, when we again have $v_v = v_v^\star$ and $T = 2693$ K. Curve (c) is for the time when a period equal to the emission duration (i.e., $t_f - t_i \simeq 12.5$ ns) has passed since the end of the emission, namely, $t = 39.9$ ns. A single LOC formally analogous to the second LOC of Fig. 7 is seen to be present.

In curve (b), at the end of the emission phase, when we have $v_v = v_v^\star$ and $t = t_f = t_v^\star = 27.4$ ns, no important differences with respect to the previous case are observed even if the flow velocity ($u_K = 404$ m/s) and density of the gas ($\rho_K = 78\,\mu$g /cm^3) at the KL boundary are a bit lower. We would point out that analytical descriptions of the problem [26,27] normally do not have a regime similar to curve (b) because they assume an instantaneous onset and ending of the emission.

Finally, in curve (c) at $t = 39.9$ ns, the density and flow velocity display a line of contact (LOC), which is a remembrance of the abrupt density drop that occurs at the end of the emission. For short enough times this LOC coincides with the absolute density maximum. Near the surface the velocity exhibits negative values due to the recondensation process. These results are very similar to those found for one-dimensional expansions based on the Boltzmann equation [18], as well as for solutions based on the gas-dynamic equations [26,27]. At 39.9 ns some 6.7% of the emitted gas has already recondensed, a quantity to be compared with 2.4–5.2% for $t = 2\,\tau_l$–$4\,\tau_l$ for a "top-hat" laser pulse [28].

Figure 6 shows a comparison between densities and flow velocities with recondensation and reflection boundary conditions for backstreaming within the KL. The

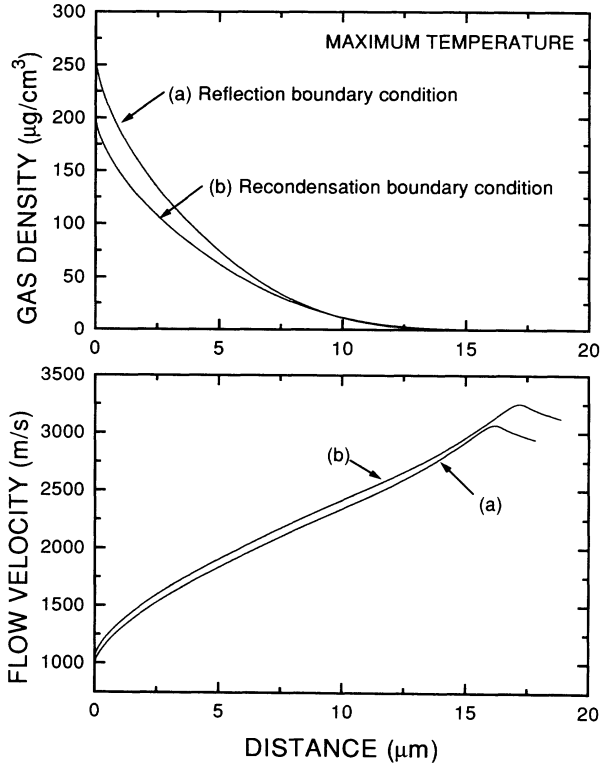

FIG. 6. Profiles of gas density and flow velocity for an energy density equal to 3.70 J/cm^2 at the time when the surface temperature is at its maximum, namely, $t = 20.3$ ns. Curve (a) corresponds to a KL with a reflection boundary condition for the backstreaming and curve (b) corresponds to a KL with a recondensation boundary condition.

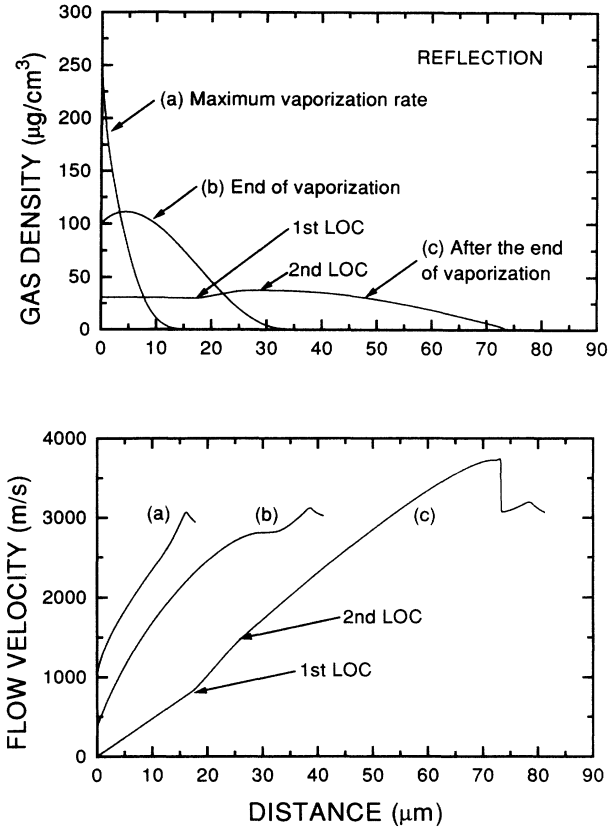

FIG. 7. Profiles of gas density and flow velocity for an energy density equal to 3.70 J/cm^2, three values of t, a reflection boundary condition, and the assumption that boiling is *not possible*. Emission leading to a UAE is found to begin at $t_i = t_v^* = 14.9$ ns, when we have $v_v = v_v^*$ and $T = 2693$ K. Curve (a) corresponds to the time when the surface temperature is at its maximum, namely, $t = 20.3$ ns. Curve (b) is for the time at the end of the emission, namely, $t_f = t_v^* = 27.4$ ns when we again have $v_v = v_v^*$ and $T = 2693$ K. Curve (c) is for the time when a period equal to the emission duration (i.e., $t_f - t_i \simeq 12.5$ ns) has passed since the end of the emission, namely, $t = 39.9$ ns. Two LOC's are seen to be present.

temperature of the sample has been taken as being at its maximum. In this situation there are no strong differences even if, in the case of a reflection boundary condition, ρ_K is a bit higher. Even the temperature profile of the surface is not significantly affected by the differences in C_{bs}: at the maximum the difference in temperature is less than 2 K.

Figure 7 shows the results obtained when reflection instead of recondensation is assumed. Although curves (a) and (b) are almost the same as the corresponding curves of Fig. 5, curve (c) shows three important differences. First, for all times the flow velocity at the surface is 0. Second, two LOC's are present both in the flow velocity and in the density profile. Third, the density exhibits a plateau between the surface and the first LOC. This is rigorously true only for atoms, but is always approximately true [26,27].

CONCLUSIONS

We have described a laser sputtering process as it would occur in a thermal regime when both a primary mechanism (due to absorption of the laser pulse) and a secondary mechanism (gas dynamics) are taken into account. In particular the following physical quantities were computed: (a) surface temperature as a function of time and with the postulate that boiling either is or is not possible on a 30 ns time scale (Fig. 1 and Table II); (b) duration of the liquid phase at the surface and duration of boiling (Table II); (c) surface recession velocity due to the vaporization process (Figs. 2–4 and Table II); (d) the crater depth (Table II); and (e) density and flow velocity of the emitted particles as a function of time with the assumption that the gas-dynamic equations (rather than the Boltzmann equation) may be adopted (Figs. 5–7).

In spite of there being only a limited possibility of direct comparison with experimental results, due both to the lack of published data (crater depth for instance) and to the difficulty in imaging the gas cloud, qualitative agreement with previous theoretical work was found [18,26–28]. The latter, however, involved rather heavy restrictions in the choice of boundary conditions. As a result the flow velocity assumed a rather simple structure given by a single straight line during the vaporization and by either two or three nearly straight lines after the end of the vaporization. On the contrary, the boundary conditions used in our model are less restrictive, the flow velocity and gas density (Figs. 5–7) being free to follow the temperature changes of the sample surface (Fig. 1). This implies a more structured flow velocity function, which departs from having straight or nearly straight components.

Even our approach, however, is not methodologically perfect. We have had to adjust the ratio p/ρ_g^γ for each value of t.

The scheme adopted here for describing laser sputtering may be improved by taking into account the temperature and phase dependence of the density, reflection and absorption coefficients, specific heat, conductivity, and heat of vaporization. Likewise, the heat input into the gas should have been considered.

A deeper understanding of the boiling mechanism is necessary to overcome our "hybrid" description of vaporization and boiling, which are supposed to happen at a pressure of 1 atm, and the gas expansion, which is supposed to be into vacuum.

Despite these possible improvements the results we have obtained should describe well enough the laser ablation process at rather low CPU expense. Indeed the study of the whole process described here required more or less 90 h of VAX6320 computer CPU time. This time applies to a situation in which the spatial and time steps were, respectively, $\Delta x \simeq 23$ nm and $\Delta t \simeq 2$ ps for the integration of the heat flow equation and $\Delta x \simeq 4$ nm and $\Delta t \simeq 0.1$ ps for the integration of the gas-dynamic equations.

At the same time the model is quite general. The laser ablation of other materials may be described simply by providing alternative parameters for Table I.

APPENDIX A: THE KNUDSEN LAYER WITH A RECONDENSATION BOUNDARY CONDITION

Here we indicate briefly how the properties at the Knudsen layer (KL) boundary can be derived when the sticking coefficient applicable to backstreaming particles is given by $C_S' = 1$, i.e., for a recondensation boundary condition. Historically the argument was pioneered by Ytrehus [29] and Cercignani [16].

Neglecting the KL thickness but requiring mass, momentum, and energy to be conserved across the layer, the following equations are obtained:

$$\rho_K u_K = \rho_S \left(\frac{k_B T_S}{2\pi m}\right)^{\frac{1}{2}} + \beta \rho_K \left(\frac{k_B T_K}{2\pi m}\right)^{\frac{1}{2}} [\alpha \pi^{\frac{1}{2}} \operatorname{erfc}(\alpha) - e^{-\alpha^2}], \quad \text{(A1)}$$

$$\rho_K u_K \left(\frac{1}{2}u_K^2 + \frac{k_B T_K}{m}\frac{\gamma}{\gamma-1}\right) = \rho_S \frac{k_B T_S}{m}\left(\frac{k_B T_S}{2\pi m}\right)^{\frac{1}{2}}\left(\frac{\gamma+1}{2(\gamma-1)}\right) + \beta \rho_K \frac{k_B T_K}{m}\left(\frac{k_B T_K}{2\pi m}\right)^{\frac{1}{2}}\left[\alpha\left(\alpha^2 + \frac{\gamma}{(\gamma-1)}\right)\pi^{\frac{1}{2}} \times \operatorname{erfc}(\alpha) - e^{-\alpha^2}\left(\alpha^2 + \frac{\gamma+1}{2(\gamma-1)}\right)\right]. \quad \text{(A3)}$$

Here α is given by $\alpha = M(\gamma/2)^{1/2}$ and ρ_s is the saturated vapor mass density at T_s.

From Eqs. (A1)—(A3), the following jump conditions [holding for $0 \le M \le 1$ (Appendix C)] may be deduced:

$$\frac{T_K}{T_S} = \left\{\left[1 + \pi\left(\frac{\gamma-1}{\gamma+1}\frac{\alpha}{2}\right)^2\right]^{\frac{1}{2}} - \pi^{\frac{1}{2}}\frac{\gamma-1}{\gamma+1}\frac{\alpha}{2}\right\}^2, \quad \text{(A4)}$$

$$\frac{\rho_K}{\rho_S} = \frac{n_K}{n_S} = \left(\frac{T_S}{T_K}\right)^{\frac{1}{2}}\left[\left(\alpha^2 + \frac{1}{2}\right)e^{\alpha^2}\operatorname{erfc}(\alpha) - \frac{\alpha}{\pi^{\frac{1}{2}}}\right] + \frac{1}{2}\frac{T_S}{T_K}\left[1 - \pi^{\frac{1}{2}}\alpha e^{\alpha^2}\operatorname{erfc}(\alpha)\right], \quad \text{(A5)}$$

$$\beta = \left[(2\alpha^2+1) - \alpha\left(\frac{\pi T_S}{T_K}\right)^{\frac{1}{2}}\right]e^{\alpha^2}\frac{\rho_S}{\rho_K}\left(\frac{T_S}{T_K}\right)^{\frac{1}{2}}, \quad \text{(A6)}$$

and

$$u_K = M a_K = M\left(\gamma\frac{k_B T_K}{m}\right)^{\frac{1}{2}}. \quad \text{(A7)}$$

Here a_K is the local sound speed at the KL boundary, and $M = u/a$ is the Mach number for a one-dimensional flow.

Furthermore, from Eqs. (A1) the backstreaming coefficient C_{bs0} as used in Eq. (14) may be deduced very simply:

$$C_{\text{bs0}} = \frac{(\text{total flux}) - (\text{escaping flux})}{(\text{total flux})} = \frac{\rho_S\left(\frac{k_B T_S}{2\pi m}\right)^{1/2} - \rho_K u_K}{\rho_S\left(\frac{k_B T_S}{2\pi m}\right)^{1/2}} = 1 - M\frac{\rho_K}{\rho_S}\left(2\pi\gamma\frac{T_K}{T_S}\right)^{1/2}. \quad \text{(A8)}$$

APPENDIX B: REFLECTION BOUNDARY CONDITION

With a reflection boundary condition (sticking coefficient given by $C_S' = 0$) and neglecting the KL thickness, the backstreaming should not change the mass and the energy fluxes between the surface and the KL boundary. Equations (A1) and (A3) therefore need to be replaced respectively by

$$\rho_K u_K = \rho_S \left(\frac{k_B T_S}{2\pi m}\right)^{\frac{1}{2}} \quad \text{(B1)}$$

and

$$\rho_K u_K \left(\frac{1}{2}u_K^2 + \frac{k_B T_K}{m}\frac{\gamma}{\gamma-1}\right) = \rho_S \frac{k_B T_S}{m}\left(\frac{k_B T_S}{2\pi m}\right)^{\frac{1}{2}}\left(\frac{\gamma+1}{2(\gamma-1)}\right). \quad \text{(B2)}$$

In regard to the linear momentum flux, in the reflection case the surface acts on the backstreaming particles as a negative-to-positive "linear momentum converter." Equation (A2) must therefore be replaced by

$$\rho_K\left(u_K^2+\frac{k_B T_K}{m}\right) = \frac{1}{2}\rho_S\frac{k_B T_S}{m}+2\beta\rho_K\frac{k_B T_K}{m} \times\left[\left(\alpha^2+\frac{1}{2}\right)\operatorname{erfc}(\alpha)-\frac{1}{\pi^{\frac{1}{2}}}\alpha e^{-\alpha^2}\right]. \tag{B3}$$

The jump conditions, in this case, may be deduced using only Eqs. (B1) and (B2):

$$\frac{T_K}{T_S}=\frac{\gamma+1}{2}\left[(\gamma-1)\alpha^2+\gamma\right]^{-1}=\frac{1}{\gamma} \tag{B4}$$

and

$$\frac{\rho_K}{\rho_S}=\frac{1}{2\alpha\pi^{1/2}}\left(\frac{T_S}{T_K}\right)^{1/2}=\frac{1}{(2\pi)^{1/2}}\,, \tag{B5}$$

where the final values correspond to $M=1$. Obviously the new value of C_{bs0} is given by $C_{\mathrm{bs0}}=0$ and the coefficient β ($\beta\neq 0$) is not needed. A discussion of the KL for conditions of reflection apparently has not been made previously.

APPENDIX C: THE HYPOTHESIS $M=1$

We show here that the condition $M=1$ is required when the flow conditions at the KL boundary are stationary. If the Poisson equation [Eq. (23b)] and the relation seen in Eq. (23c) are used, then Eqs. (21a) and (21b) can be rewritten as

$$\frac{\partial a}{\partial t}+u\frac{\partial a}{\partial x}+\frac{(\gamma-1)\,a}{2}\frac{\partial u}{\partial x}=0\,, \qquad \frac{\partial u}{\partial t}+u\frac{\partial u}{\partial x}+\frac{2\,a}{\gamma-1}\frac{\partial a}{\partial x}=0. \tag{C1}$$

Then "stationary" or "almost stationary" flow at the KL boundary means

$$\left.\frac{\partial u}{\partial t}\right|_K\simeq\left.\frac{\partial a}{\partial t}\right|_K\simeq 0 \tag{C2}$$

and we have

$$u\frac{\partial a}{\partial x}+\frac{(\gamma-1)\,a}{2}\frac{\partial u}{\partial x}\simeq 0\,, \qquad u\frac{\partial u}{\partial x}+\frac{2\,a}{\gamma-1}\frac{\partial a}{\partial x}\simeq 0. \tag{C3}$$

Equations (C3) can be rearranged to

$$\frac{(\gamma-1)\,u}{2\,a}\simeq\frac{(\gamma-1)\,a}{2\,u}, \tag{C4}$$

from which follow the relations $u_K\simeq a_K$ and $M\simeq 1$.

This simple argument has apparently not been made previously. Rather, much more complicated derivations were used [16,29].

[1] N. Bloembergen, H. Kurz, J. M. Liu, and R. Yen, in *Laser and Electron-Beam Interactions with Solids,* edited by B. R. Appleton and G. K. Celler (Elsevier Science, New York, 1982), p. 3.

[2] M. M. Martynyuk, Zh. Tekh. Fiz. **46**, 741 (1976) [Sov. Phys. Tech. Phys. **21**, 430 (1976)].

[3] D. L. Lin, X. Li, and T. F. George, Mat. Sci. Eng. B **23**, L9 (1994).

[4] R. Kelly, A. Miotello, B. Braren, A. Gupta, and K. Casey, Nucl. Instrum. Methods **B65**, 187 (1992)

[5] V. A. Batanov, F. V. Bunkin, A. M. Prokhorov, and V. B. Fedorov, Zh. Eksp. Teor. Fiz. **63**, 586 (1972) [Sov. Phys. JETP **36**, 311 (1973)].

[6] J. Lin and T. F. George, J. Appl. Phys. **54**, 382 (1983).

[7] H. S. Carslaw and J. C. Jaeger, *Conduction of Heat in Solids* (Oxford University Press, Oxford, 1959), p. 50.

[8] R. E. Harrington, J. Appl. Phys. **38**, 3266 (1967)].

[9] L. F. Donà dalle Rose and A. Miotello, in *European Scientific Laser Workshop on Mathematical Simulation,* edited by H.W. Bergmann (Sprechsaal, Coburg, 1989), p. 242.

[10] S. Williamson, G. Morou, and J. C. M. Li, Phys. Rev. Lett. **52**, 2364 (1984).

[11] G. M. Pound, J. Phys. Chem. Ref. Data **1**, 135 (1972).

[12] J. P. Hirth and G. M. Pound, J. Phys. Chem. **64**, 619 (1960).

[13] F. V. Bunkin and M. I. Tribel'skiĭ, Usp. Fiz. Nauk **130**, 193 (1980) [Sov. Phys. Usp. **23**, 105 (1980)].

[14] R. Kelly, J. Chem. Phys. **92**, 5047 (1990).

[15] R. Kelly and R. W. Dreyfus, Surf. Sci. **198**, 263 (1988).

[16] C. Cercignani, in *Rarefied Gas Dynamics*, edited by S. S. Fisher (AIAA, New York, 1981), p. 305.

[17] K. L. Saenger, J. Chem. Phys. **75**, 2467 (1981).

[18] D. Sibold and H. M. Urbassek, Phys. Rev. A **43**, 6722 (1991).

[19] I. NoorBatcha, R. R. Lucchese, and Y. Zeiri, J. Chem. Phys. **86**, 5816 (1987).

[20] I. NoorBatcha, R. R. Lucchese, and Y. Zeiri, J. Chem. Phys. **89**, 5251 (1988).

[21] F. Reif, *Fundamentals of Statistical and Thermal Physics* (McGraw-Hill, Tokyo, 1965), p. 516.

[22] H. M. Urbassek and J. Michl, Nucl. Instrum. Methods Phys. Res. Sec. B **22**, 480 (1987).

[23] S. Chapman and T. G. Cowling, *The Mathematical Theory of Non-Uniform Gases* (Cambridge University Press, Cambridge, 1970).

[24] J. H. Ferziger and H. G. Kaper, *Mathematical Theory of Transport Processes in Gases* (North-Holland, Amsterdam, 1972), p. 107.
[25] S. K. Godunov, A. V. Zabrodin, and G. P. Prokopov, U.S.S.R. Comput. Math. Math. Phys. **4**, 1187 (1962).
[26] R. Kelly and A. Miotello, Appl. Phys. B **57**, 145 (1993).
[27] D. Sibold and H. M. Urbassek, Phys. Fluids A **4**, 165 (1992).
[28] R. Kelly and A. Miotello, Nucl. Instrum. Methods Phys. Res. Sec. B **91**, 682 (1994).
[29] T. Ytrehus, in *Rarefied Gas Dynamics*, edited by J. L. Potter (AIAA, New York, 1977), p. 1197.